Universal distribution of magnetic anisotropy of impurities in ordered and disordered nanograins

A. Szilva,[1,2] P. Balla,[2,3] O. Eriksson,[1] G. Zaránd,[4] and L. Szunyogh[2,5]

[1]*Department of Physics and Astronomy, Division of Materials Theory, Uppsala University, Box 516, SE-75120 Uppsala, Sweden*

[2]*Department of Theoretical Physics, Budapest University of Technology and Economics, Budafoki út 8, H-1111 Budapest, Hungary*

[3]*Institute for Solid State Physics and Optics, Wigner Research Centre for Physics, Hungarian Academy of Sciences, P.O. Box 49, H-1525 Budapest, Hungary*

[4]*BME-MTA Exotic Quantum Phases "Lendület" Group, Institute of Physics, Budapest University of Technology and Economics, H-1521 Budapest, Hungary*

[5]*MTA-BME Condensed Matter Research Group, Budapest University of Technology and Economics, Budafoki út 8, H-1111 Budapest, Hungary*

(Received 22 January 2015; revised manuscript received 20 March 2015; published 20 April 2015)

We examine the distribution of the magnetic anisotropy experienced by a magnetic impurity embedded in a metallic nanograin. As an example of a generic magnetic impurity with a partially filled d shell, we study the case of d^1 impurities embedded into ordered and disordered Au nanograins, described in terms of a realistic band structure. Confinement of the electrons induces a magnetic anisotropy that is large, and can be characterized by five real parameters, coupling to the quadrupolar moments of the spin. In ordered (spherical) nanograins, these parameters exhibit symmetrical structures and reflect the symmetry of the underlying lattice, while for disordered grains they are randomly distributed and, for stronger disorder, their distribution is found to be characterized by random matrix theory. As a result, the probability of having small magnetic anisotropies K_L is suppressed below a characteristic scale Δ_E, which we predict to scale with the number of atoms N as $\Delta_E \sim 1/N^{3/2}$. This gives rise to anomalies in the specific heat and the susceptibility at temperatures $T \sim \Delta_E$ and produces distinct structures in the magnetic excitation spectrum of the clusters that should be possible to detect experimentally.

DOI: 10.1103/PhysRevB.91.134421 PACS number(s): 75.30.Hx, 73.21.−b, 73.22.−f, 75.30.Gw

I. INTRODUCTION

Magnetic thin films and nanosized objects are essential ingredients for high-density magnetic recording. Magnetic nanoparticles, in particular, are considered as the most likely building blocks for future permanent magnets [1–3]. Similar to molecular electronics devices [4] or thin metallic layers [5,6], spin-orbit (SO) coupling plays an essential role in nanoparticles: By restricting the free motion of the magnetic spins and eventually freezing them [7], it enables spins to store magnetic information. Understanding the behavior of the magnetic anisotropy in systems with quantum confinement is hence of crucial importance for nanoscale magnetic materials science.

SO coupling-induced magnetic anisotropy (MA) appears to be surprisingly large in certain nanoscale and mesoscopic structures. A sterling example, where confinement-induced MA provides an explanation for the observation, is the suppression of the Kondo effect in thin films and wires of certain dilute magnetic alloys [5]. As revealed by a series of experiments on magnetically doped thin metallic films [5,6], SO coupling combined with a geometrical confinement of the electrons' motion induces a "dead layer" in the vicinity of the surface, where the motion of the otherwise free spins is blocked by MA. The thickness d of this "dead layer," consistently explained in terms of surface-induced spin anisotropy [5,6], depends on the particular host material and dopants used, but it can be unexpectedly large, in the range of $d \sim 100$ Å.

In confined geometries, a spin-orbit (SO) interaction can induce magnetic anisotropies by two fundamentally different mechanisms. In metallic compounds of heavy elements with a strong SO interaction, the geometry of the sample is imprinted into the spin texture of the *conduction electrons*' wave function. This spin texture varies in space close to the surface of the sample, and induces a position dependent magnetic anisotropy for the magnetic dopants. The corresponding host-induced magnetic anisotropy host SO (HSO) mechanism, intensively studied in atomic-scale engineering, is presumably at work in magnetically doped noble metal samples, where it gives rise to a relatively short-ranged confinement-induced magnetic anisotropy close to the sample surfaces [7]. Much stronger and longer-ranged anisotropy can, however, be generated by the local SO (LSO) coupling at the magnetic dopant's d or f level [8,9] in the case of magnetic impurities with a partially filled d or f shell, respectively [8]. In this case, the spin of the magnetic ion is entangled with the orbital structure of localized f and d states, and couples very strongly to Friedel oscillations, leading to the emergence of a strong MA (LSO mechanism). While the HSO mechanism appears to be too weak to explain the thin film experiments, the stronger and more slowly decaying anisotropy induced by the LSO mechanism seems to give a consistent explanation for the experimental observations [8–10], and appears to be the dominant mechanism for SO coupling-induced MA in confined structures.

The surface-induced MA has been thoroughly studied in thin films and in the vicinity of surfaces. Surprisingly little is known, however, about the structure and size of confinement-induced MA in nanograins. Here we therefore investigate the LSO mechanism in metallic grains and demonstrate that symmetrically "ordered" nanograins and nanograins with random surfaces show very different behaviors. In ordered nanograins, the MA constants exhibit regular structures reflecting the symmetry of the grain. Different atomic shells of the grain behave very differently from the point of view of magnetic anisotropy, which displays Friedel-like shell-to-shell oscillations. Adding atoms to an ordered grain and thereby

making its surface disordered, however, changes this picture completely: In such "disordered" grains, the conduction electron's wave function becomes chaotic, and the distribution of MA parameters becomes gradually more and more random. The MA distribution is then found to be fairly well captured by random matrix theory, and to be almost independent of the magnetic ion's position.

II. MODEL AND COMPUTATIONAL DETAILS

In the present work, we shall demonstrate the characteristic properties discussed above by focusing on the simplest case of a magnetic impurity in a d^1 configuration embedded into an fcc Au nanograin host of 100–400 atoms. This model system captures the generic properties of most magnetic impurities and hosts, and allows us to study the roles of local and host SO interactions simultaneously. We construct the nanograins by placing Au atoms on a regular fcc lattice starting from a central site, and then adding "shells," defined as groups of atoms that transform into each other under the cubic group (O_h). We refer to nanograins with only filled shells as *ordered* (or spherical) nanograins, while nanograins with partially filled outermost shells shall be referred to as *disordered* (or nonspherical) nanoparticles. We also define the *core* of the grain as the group of atoms having a complete set of first neighbors. To describe the electronic structure of Au nanograins, we use a tight binding model with *spd* canonical orbitals and incorporate SO coupling of the host atoms nonperturbatively. More technical details can be found in Appendix A.

To investigate the local SO-induced anisotropy, we shall use the approach of Ref. [11], and account for local correlations on the magnetic impurity by means of a generalized Anderson model [12], which we embed into the Au grain described above. Similar to Anderson's model, our impurity Hamiltonian (the so-called ionic model [13]) contains three terms: the impurity term, the conduction electron, and the hybridization terms (see Appendix B). In the ground state d^1 configuration, by Hund's third rule, the strong local SO interaction aligns the angular momentum of the d electron antiferromagnetically with its spin, thus forming a $D^{3/2}$ spin $j = 3/2$ multiplet. This multiplet remains degenerate in a perfect cubic environment, and—in group theoretical terms—it transforms according to the four-dimensional Γ_8 double representation of the cubic point group [14].

Next, we need to embed this impurity into the host. Following Anderson, we consider hybridization of the deep $D^{3/2}$ multiplet only with s-type host electrons, since these latter dominate the density of states near the Fermi energy (see Appendix B). Local cubic symmetry implies, however, that only linear combinations of neighboring s orbitals, transforming as $j \sim 3/2$, can hybridize with the deep $D^{3/2}$ states. The proper $|s_{3/2}\rangle$, $|s_{1/2}\rangle$, $|s_{-1/2}\rangle$, $|s_{-3/2}\rangle$ basis set has been constructed in Refs. [10,11] and is reproduced in Appendix B. Considering then charge fluctuations to the d^0 state and performing a Coqblin-Schrieffer transformation [15,16], we finally arrive at the following simple exchange Hamiltonian,

$$\mathcal{H}_{\rm LSO} = J \sum_{m,m'} s^\dagger_m s_{m'} |m'\rangle\langle m|. \tag{1}$$

Here the $\{|m\rangle\}$ refer to the states $\{\frac{3}{2}, \frac{1}{2}, -\frac{1}{2}, -\frac{3}{2}\}$ of the impurity, and $s^\dagger_m$ creates appropriate host electrons, while J denotes the strength of the effective exchange coupling (see also Appendix B).

To handle the exchange interaction J, we can use a diagrammatic approach similar to Ref. [11]. The dominant contribution to the MA is, however, simply given by the Hartee term, generating the effective spin Hamiltonian,

$$H^L = \sum_{m,m'} K_{mm'} |m'\rangle\langle m|,$$

with the anisotropy matrix $K_{mm'}$ expressed as

$$K_{mm'} = J\langle s^\dagger_m s_{m'}\rangle = J \int_{-\infty}^{\varepsilon_F} d\varepsilon\, \rho^L_{mm'}(\varepsilon). \tag{2}$$

Here $\rho^L(\varepsilon)$ denotes the local spectral function matrix of the symmetry adapted host operators $s^\dagger_m$ and ε_F stands for the Fermi energy. In practice, we evaluate the integral (C6) in terms of the Green's functions of the host [17].

III. SYMMETRY CONSIDERATIONS

Although disordered nanograins do not possess spatial symmetries, time reversal (TR) symmetry is still present, and implies that, apart from an unimportant overall shift K_0, the anisotropy matrix $K_{mm'}$ can be parametrized in terms of five real numbers K_μ ($\mu = 1 \ldots 5$),

$$\begin{pmatrix} K_1 & K_3 - iK_5 & K_2 - iK_4 & 0 \\ K_3 + iK_5 & -K_1 & 0 & K_2 - iK_4 \\ K_2 + iK_4 & 0 & -K_1 & -K_3 + iK_5 \\ 0 & K_2 + iK_4 & -K_3 - iK_5 & K_1 \end{pmatrix}, \tag{3}$$

which we shall refer to as the LSO-MA parameters. We note that the absence of SO coupling on the host atoms further simplifies the structure of H^L, and the matrix elements K_3, K_4, and K_5 vanish in the case where the up and down spin channels do not mix in the host.

The MA matrix in Eq. (3) has two Kramers degenerate eigenvalues, $\lambda_+ = -\lambda_-$, whose splitting can be used to define naturally the *magnetic anisotropy constant* as

$$K_L \equiv (\lambda_+ - \lambda_-)/2 = \sqrt{\sum_\mu K_\mu^2}. \tag{4}$$

If the magnetic impurity is placed in an ordered (spherical) nanograin, then the MA matrices can be different for different sites even if they belong to the same shell. Their trace, eigenvalues, and, therefore, the MA constant should, however, be the same for all sites within the same shell due to the underlying (O_h) symmetry of the grain, as indeed confirmed by our numerical simulations, discussed below (for additional information, see Appendix C).

To find connections between the elements of $K_{mm'}$ for an ordered nanograin, we express Eq. (3) in a multipolar basis. Time reversal symmetry implies that $K_{mm'}$ can be expressed solely in terms of even powers of the $j = 3/2$ spin operators

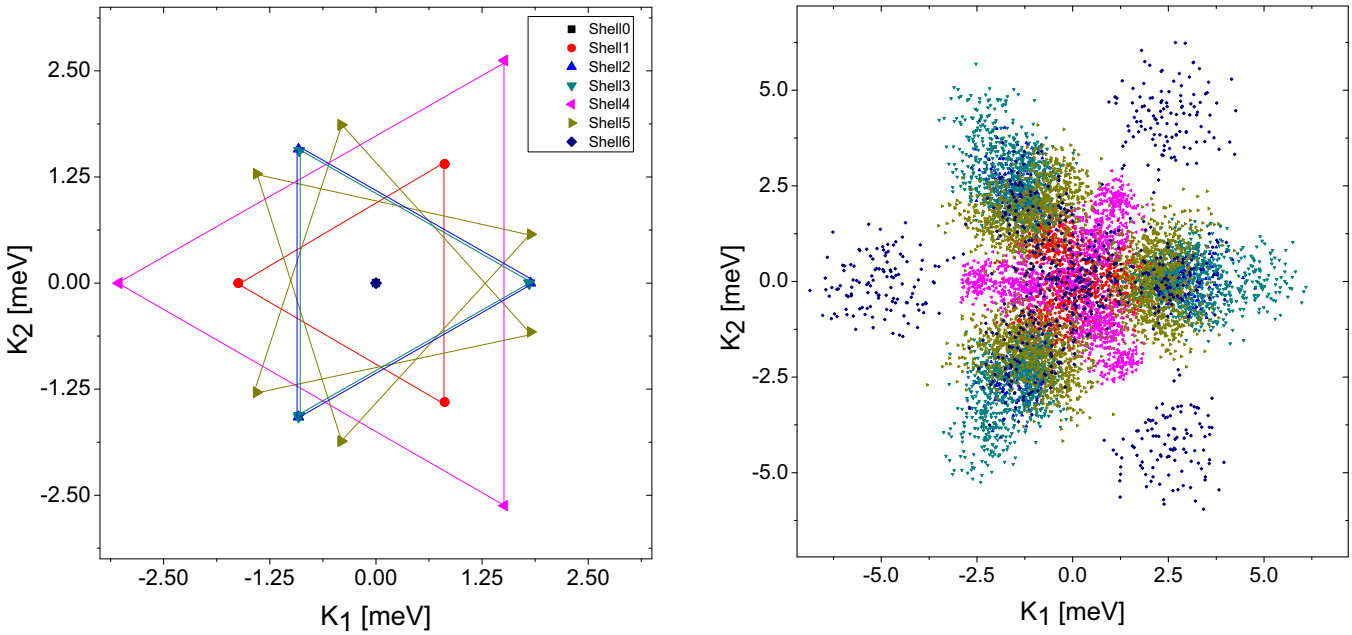

FIG. 1. (Color online) Left: Anisotropy parameters in the E plane for an ordered grain of 225 atoms (87 core atoms). Right: Anisotropies in the E plane in case of 100 disordered Au nanograins. An ordered cluster is created by 225 atoms that fill completely the first six shells of the fcc structure, and with 11 extra atoms, randomly placed onto the next shell. The triangular structure of the anisotropy parameter distribution can still be observed.

J_x, J_y, J_z. In fact, the parameters in (3) couple directly to the usual five (normalized and traceless) quadrupole operators allowed by time reversal symmetry, $Q_1, \ldots, Q_5$ proportional to $2J_z^2 - J_x^2 - J_y^2$, $J_x^2 - J_y^2$, $J_xJ_z + J_zJ_x$, $J_xJ_y + J_yJ_x$, and $J_yJ_z + J_zJ_y$, respectively. The local Hamiltonian can be simply expressed in terms of these as

$$H^L = \sum_\mu K_\mu Q_\mu, \tag{5}$$

with the coefficients K_μ of the Q matrices forming a five-dimensional vector. Under cubic point group transformations, the first two components, $\sim(Q_1, Q_2)$, and the last three components, $\sim(Q_3, Q_4, Q_5)$, transform into each other according to the E and T_2 representations of the cubic point group, respectively [14]. Correspondingly, for atoms on the same shell of an ordered grain, the anisotropy parameters $K_{1,2}$ transform into each other, and form regular patterns of triangular symmetry in the (K_1, K_2) plane, referred to as the E plane in what follows. The left panel of Fig. 1 shows the computed (K_1, K_2) values, plotted in the E plane for an ordered grain of 225 atoms (87 core atoms). Throughout this work, we use $J = 0.25$ eV, a value consistent with a Kondo temperature below 0.1 K. Different colors denote the MA parameters of clusters with magnetic impurities placed on the different shells. Similarly, the anisotropy constants K_3, K_4, and K_5 (shown in Fig. 7 in Appendix C), induced by the SO interaction on the *host* Au atoms, are related for atoms on the same shell, and show regular patterns in a three-dimensional space, the T_2 space. These parameters are, however, smaller by about one order of magnitude compared to the parameters $K_{1,2}$, implying that the MA constant, Eq. (4), is dominated by the E-type parameters.

IV. ANALYSIS OF DISORDERED CLUSTERS

Next, let us examine the distribution of the magnetic anisotropy constants in case of disordered nanoclusters. First, we created 100 disordered nanoclusters by adding 11 extra atoms to an 225-atom ordered cluster, and placing them randomly on the next shell of 24 possible sites. We then calculated the MA parameters on all core sites for every nanoparticle. In Fig. 1 (right) we show the 8700 E-plane parameters obtained this way. Different colors represent data from different shells. Small "clouds" are observed with obvious remains of the threefold symmetry, but there is no longer any strictly ordered structure left in the E plane.

We then increased the structural disorder of the nanograins further, and added 25 extra atoms to an ordered cluster of 225 atoms, by placing them randomly on the next three shells. As shown in the inset of Fig. 2, for these strongly disordered clusters the distribution becomes almost isotropic in the E plane, and the triangular symmetry is almost entirely lost. The main panel of Fig. 2 shows the radial distribution of the magnetic anisotropy parameters, $\sqrt{K_1^2 + K_2^2}$ in the E plane. The observed distribution agrees very well with the predictions of a simple Gaussian theory, where the components of $\mathbf{K}_E \equiv (K_1, K_2)$ have an independent and Gaussian distribution,

$$p(\mathbf{K}_E) \sim e^{-\mathbf{K}_E^2/\Delta_E^2}, \tag{6}$$

with the E-plane anisotropy scale Δ_E defined as $\Delta_E^2 \equiv \langle \mathbf{K}_E^2 \rangle$. We find that in these disordered grains the radial distribution in the three-dimensional T_2-space parameters can also be fitted by a similar Gaussian ensemble, although with a smaller characteristic radius, $\sqrt{\langle \mathbf{K}_T^2 \rangle} \equiv \Delta_T < \Delta_E$ (see Fig. 8 in Appendix C). The overall distribution of the anisotropy K_L is therefore strongly suppressed at small values. In the

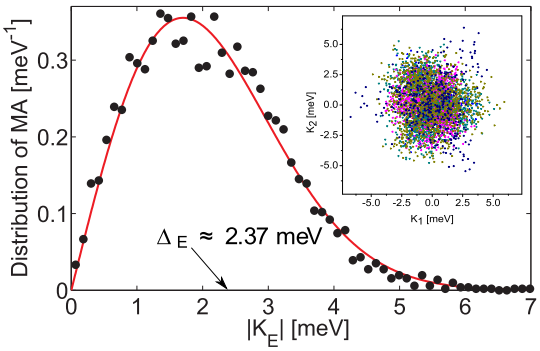

FIG. 2. (Color online) Radial distribution of the magnetic anisotropy parameters (dots) in the E plane in the case of $N_S = 50$ samples with $N = 225 + 25$ atoms. The continuous line presents the predictions of the Gaussian orthogonal ensemble. Inset: Distribution of (K_1, K_2) in the E plane for these 50 nanograins. At this level of disorder the triangular structure is almost entirely lost.

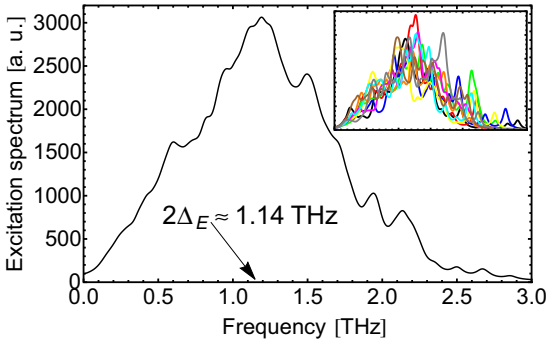

FIG. 3. (Color online) Orientational and disorder averaged excitation spectrum computed for an ensemble of 1000 randomly chosen and randomly oriented disordered nanograins ($N = 225 + 40$). The shape of the signal reflects the distribution of magnetic anisotropies while the small peak corresponds to transitions between the lowest Kramers doublets, split by the magnetic field. Inset: Spectra of selected grains, see the main text and Appendix E.

absence of host SO coupling, it scales as $p(K_L) \sim K_L$ for small anisotropy values, $K_L < \Delta_E$, while in the presence of it $p(K_L)$ is suppressed as $p(K_L) \sim |K_L|^4$ for $K_L < \Delta_T$. This implies that *typical* sites in a disordered grain have a *finite* SO-induced anisotropy of size $\sim\Delta_E$, and of random orientation, almost independently of their precise location within the grain.

We remark that, even after adding a single extra atom to an ordered cluster, the distribution of the eigenenergies of the host Hamiltonian agreed with the predictions of random matrix theory (see Fig. 9 in Appendix D) and, in agreement with the experimental findings [18], exhibited level repulsion according to a Gaussian symplectic (GS) level spacing distribution. The observed GS distribution reflects the chaotic nature of the electron's wave function as well as the presence of *host* SO coupling. Building upon the chaotic nature of the electron's wave function, one can obtain an estimate of Δ_E by using Eq. (C6) and assuming random plane wave conduction electron wave functions [19]. This yields the estimate

$$\Delta_E \sim J(\Delta_{\rm SO}/\epsilon_F)/N^{3/2},$$

with N the number of lattice sites on the cluster and $\Delta_{\rm SO}$ the SO splitting of the $j = 3/2$ and $j = 5/2$ impurity levels.

V. EXPERIMENTAL IMPLICATIONS

The anisotropy distribution (6) has a direct impact on the magnetic excitation spectrum of the nanograins. Generating 50 (strongly) disordered nanograins with $225 + 40$ atoms (87 core sites), we randomly chose and rotated 100 nanoclusters from the 4350 different samples (see Appendix E), and determined the magnetic impurities' excitation spectrum averaging over the orientation of them. All these 100 spectra were added together, and the procedure was repeated ten times. The obtained aggregated spectrum is shown in Fig. 3. The obtained spectra are grain specific (see the inset), and reflect directly the MA energy's distribution. The typical anisotropy values, $\Delta_E \approx 0.57$ THz, shift rapidly towards smaller values (GHz) with increasing grain size.

The universal anisotropy distribution should be indirectly observable through thermodynamic quantities, too. In the presence of a random distribution of anisotropies, given by Eq. (6), we obtain a peak in the specific heat $C(T)$ at $T \approx 0.78\Delta_E$, and a low temperature specific heat $C(T) \sim T^2/\Delta_E^2$ (see Appendix F), turning into a $\sim T^5$ anomaly for $T \ll \Delta_T$. It should be emphasized that the specific heat (Fig. 10 in Appendix E) is universal for all disordered nanograins, where the MA constants follow a Gaussian orthogonal ensemble (GOE) type of distribution. The grain-specific information is hidden in the parameter Δ_E. We note that the coefficient of the Curie susceptibility $\sim T\chi$ should exhibit a strong suppression below $T \sim \Delta_E$, similarly to the specific heat.

VI. CONCLUSIONS

Although the model discussed here has features that are specific, we believe that it captures many generic properties of magnetic impurities in a metallic grain, and thus allows one to draw general conclusions. For any magnetic impurity of spin J, time reversal symmetry implies that the leading anisotropy term is of the form (5). In ordered grains, the distribution of the five parameters K_μ must always reflect the underlying lattice symmetry, and for cubic lattices, in particular, the couplings $\mathbf{K}_E$ and $\mathbf{K}_T$ are organized into triangular and cubic structures, respectively. These parameters are expected to become random, and to exhibit multidimensional Gaussian distributions in sufficiently disordered grains. We have found that the MA constants K_L in nanoballs with magnetic impurities follow a universal distribution function when the structural disorder is large enough. The suppression of the probability of having a small anisotropy, $p(K_L \to 0) = 0$, as well as the predicted specific heat and susceptibility anomalies are also generic (not only GOE) features, since they follow simply from the presence of randomly distributed independent anisotropy parameters K_μ. Our conclusions regarding the Schottky anomaly are thus general, though details of the low temperature scaling of $C(T)$ may be system (MA distribution) specific.

ACKNOWLEDGMENTS

We owe thanks to Agnes Antal, Imre Varga, and Jan Rusz for the fruitful discussions. This work has been financed by the Swedish Research Council, the KAW Foundation, and the ERC (Project No. 247062-ASD) and the Hungarian OTKA Projects No. K105148 and No. K84078. We also acknowledge support from eSSENCE and the Swedish National Allocations Committee (SNIC/SNAC).

APPENDIX A: DESCRIPTION OF THE GOLD NANOGRAIN

We have defined the structure of the Au nanograins host of $N = 100$–400 atoms as follows: We refer to an *ordered* grain when it has only filled shells around a *central* atom, while nanoparticles with partially filled (outermost) shells are referred to as *disordered* nanograins. The *shell* is a group of atoms ($N_{\rm sh}$) on an fcc lattice, transforming into each other under the cubic group (O_h). The shell structure of a few fcc nanoclusters is shown in Table I. An ordered grain built by $N = 225$ atoms has, e.g., 12 filled shells: one central atom, 12 first, six second,..., and 24 twelfth neighbors. The site (0,1.5,1.5) belongs to shell $9NNa$, while the site (0.5,0.5,2) is on shell $9NNb$, though they are at the same distance from the origin (center atom). A disordered grain host of $N = 236$ atoms with 11 atoms in the outermost ($12NN$) shell (instead of $N_{\rm sh} = 24$ atoms) has, e.g., C_{11}^{24} configurations. In practice, we choose randomly only around $N_S \sim 50$–100 grains from this huge configuration space. We allow placing extra atoms not only into the first outermost shell, however, we never generate "holes" in a nanocluster. In a given nanograin the atoms that have all the first neighbors are referred to as *core* atoms (denoted by N_c in Table I). The core region is away from the surface of the nanograin. A nanoparticle of $N = 225$ atoms has, e.g., $N_c = 87$ core atoms.

The electronic structure of the Au nanograins will be described by a tight binding (TB) Hamiltonian. The model uses spd canonical orbitals, and the spin-orbit (SO) coupling of the host atoms is considered nonperturbatively. Specifically, the TB model uses (nearly) orthonormal basis functions which are localized at sites $\mathbf{R}_n$,

$$\langle \mathbf{r} \mid n;\alpha\sigma\rangle = \langle \mathbf{r}-\mathbf{R}_n \mid \alpha\sigma\rangle = \psi_\alpha(\mathbf{r}-\mathbf{R}_n)\phi_\sigma, \tag{A1}$$

where n refers to the given site, and the index α denotes the so-called canonical basis (real spherical harmonics),

$$\begin{aligned} &\alpha = s, \quad \ell = 0, \\ &\alpha = p_x, p_y, p_z, \quad \ell = 1, \\ &\alpha = d_{xy}, d_{xz}, d_{yz}, d_{x^2-y^2}, d_{3z^2-1}, \quad \ell = 2. \end{aligned} \tag{A2}$$

ψ_α depends only on the azimuthal quantum number ℓ and the spin quantum number is labeled by $\sigma = \pm\frac{1}{2}$.

The Hamiltonian of the noble metal host is written as

$$\begin{aligned} \hat{H} &= \left\{H^{n,n'}_{\alpha\sigma,\alpha'\sigma'}\right\} \\ &= \left(\varepsilon_\alpha \delta_{\alpha\alpha'}\delta_{\sigma\sigma'} + \xi H^{LS}_{\alpha\sigma,\alpha'\sigma'}\right)\delta_{nn'} + t^{n,n'}_{\alpha,\alpha'}\delta_{\sigma\sigma'}, \end{aligned} \tag{A3}$$

where the dimension of the matrix is $M = 18 \times N$. Here ε_α is the so-called on-site energy parameter,

$$H^{LS}_{\alpha\sigma,\alpha'\sigma'} = \langle \alpha\sigma | \vec{L}\vec{S} | \alpha'\sigma'\rangle, \tag{A4}$$

ξ is the SO coupling parameter, and $t^{n,n'}_{\alpha,\alpha'}$ are the hybridization matrix elements (or hopping integrals) between the different orbitals.

We note that on-site energies ε_s, ε_p, ε_{d-E_g} and $\varepsilon_{d-T_{2g}}$ have been used in all calculations, and hopping integrals to first and second nearest neighbors have been included. These latter depend only on the relative positions of the sites,

$$t^{n,n'}_{\alpha,\alpha'} = t_{\alpha,\alpha'}(\mathbf{R}_{n'} - \mathbf{R}_n). \tag{A5}$$

The numerical values for both ε_α and $t_{\alpha,\alpha'}$ can be found in Ref. [10]. The spin-orbit coupling parameter ξ was determined from the difference of the SO-split d-resonance energies

$$\Delta E_d = E_{j=5/2} - E_{j=3/2}, \tag{A6}$$

derived from self-consistent relativistic (SKKR) first-principles calculations [20]. This splitting is related to the strength of SO coupling as $\Delta E_d \simeq \frac{5}{2}\xi$. For bulk Au we thus obtain $\xi = 0.64$ eV.

The Green's function or resolvent operator of a nanoparticle is defined as

$$\hat{G}(z) = G^{n,n'}_{\alpha\sigma,\alpha'\sigma'}(z) = (z - \hat{H})^{-1} \tag{A7}$$

and can be written as

$$\hat{G}(z) = \sum_{i=1}^{M} \frac{|v_i\rangle\langle v_i|}{z - \varepsilon_i}, \tag{A8}$$

where $\{\varepsilon_i\}$ and $\{|v_i\rangle\}$ stand for the eigenvalues and eigenvectros of the Hamiltonian Eq. (A3), respectively.

We define the density of states (DOS) as follows,

$$n(\varepsilon) = -\frac{1}{2\pi i}\lim_{\delta\to 0} \mathrm{Tr}[\hat{G}(\varepsilon + i\delta) - \hat{G}(\varepsilon - i\delta)]. \tag{A9}$$

The numerically calculated values are shown in Fig. 4 for an ordered nanograin. The calculated Fermi energy is

TABLE I. The shell structure of fcc clusters. Labels a and b denote the shells where the atoms are at the same distance from the center atom but cannot be transformed into each other (under O_h). $N_{\rm sh}$ denotes the number of sites in a given shell, N is the total number of atoms, and N_c is the number of core sites in the cluster.

Shell	$N_{\rm sh}$	N	N_c	Shell	$N_{\rm sh}$	N	N_c
Center	1	1	0	$12NN$	24	249	87
$1NN$	12	13	1	$13NNa$	48	297	135
$2NN$	6	19	1	$13NNb$	24	321	141
$3NN$	24	43	1	$14NN$	48	369	165
$4NN$	12	55	13	$15NN$	12	381	177
$5NN$	24	79	19	$16NNa$	24	405	177
$6NN$	8	87	19	$16NNb$	24	429	201
$7NN$	48	135	43	$17NNa$	24	453	225
$8NN$	6	141	43	$17NNb$	6	459	225
$9NNa$	12	153	55	$18NN$	48	507	249
$9NNb$	24	177	55	$19NN$	24	531	249
$10NN$	24	201	79	$20NN$	24	555	273
$11NN$	24	225	87				

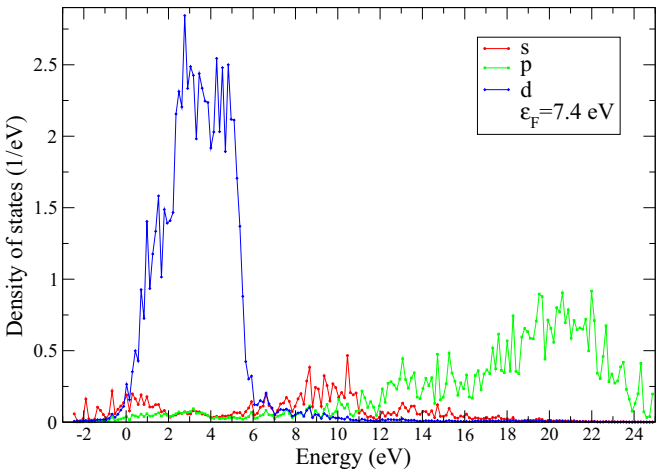

FIG. 4. (Color online) The *spd* density of states (DOS) components of an ordered nanograin ($N = 225$) normalized to one atom. The calculated Fermi energy is $\varepsilon_F = 7.4$ eV.

$\varepsilon_F = 7.4$ eV, and at the Fermi energy the s contribution dominates the DOS.

APPENDIX B: THE LSO MODEL HAMILTONIAN

Here we outline the derivation of the local spin-orbit (LSO) model for a d^1-type magnetic impurity from the so-called *ionic model*, a generalization of the Anderson model [13]. The Hamiltonian of the ionic model is constructed in terms of local crystal field multiplets of an ion, specified by the number of electrons n, some multiplet labels Γ, and internal quantum numbers m. We consider the simplest case, where the Coulomb interaction is very large, and the ground state multiplet has $n = 1$ electrons, characterized by some internal multiplet labels. In this case, quantum fluctuations to the $n = 0$ ionic state $|0\rangle$ generate the exchange interaction, and the ionic model reduces to

$$E_0|0\rangle\langle 0| + \sum_m E_1|m\rangle\langle m| + \sum_{\vec{k},m} \varepsilon_{\vec{k}} s^\dagger_{\vec{k},m} s_{\vec{k},m} + \sum_{\vec{k},m} (V_{\vec{k}}|m\rangle\langle 0|s_{\vec{k},m} + V^*_{\vec{k}} s^\dagger_{\vec{k},m}|0\rangle\langle m|), \tag{B1}$$

with m running over $2j + 1$ values. In case of $j = \frac{1}{2}$, the $U = \infty$ Anderson model is recovered [15]. The operator $s^\dagger_{\vec{k},m}$ creates a host conduction electron with wave number $\vec{k}$, pseudospin m, and energy $\varepsilon_{\vec{k}}$, adopted to the symmetry of the local ionic states $|m\rangle$, and the $V_{\vec{k}}$-s denote s-d hybridization matrix elements.

The ion experiences locally a cubic symmetry. Therefore the local art of Hamiltonian—and thus the hybridization—must be invariant under the cubic group. To construct the hybridization term, we construct symmetry-adopted combinations from the 12 operators, $s^\dagger_{xy}, s^\dagger_{\bar{x}y}, \ldots, s^\dagger_{\bar{y}\bar{z}}$, creating s electrons on nearest neighbor gold atoms. The most strongly hybridized states of d-level symmetry are the E-type combinations $D_{x^2-y^2}$ and $D_{2z^2-x^2-y^2}$ transforming as Γ_3, and are generated by the operators

$$\begin{aligned} D^\dagger_{x^2-y^2} &= \frac{1}{2\sqrt{2}}(s^\dagger_{\mathbf{yz}} + s^\dagger_{\bar{\mathbf{y}}\bar{\mathbf{z}}} + s^\dagger_{\mathbf{y}\bar{\mathbf{z}}} + s^\dagger_{\bar{\mathbf{y}}\mathbf{z}} \\ &\quad - s^\dagger_{\mathbf{xz}} - s^\dagger_{\bar{\mathbf{x}}\bar{\mathbf{z}}} - s^\dagger_{\mathbf{x}\bar{\mathbf{z}}} - s^\dagger_{\bar{\mathbf{x}}\mathbf{z}}), \\ D^\dagger_{2z^2-x^2-y^2} &= \frac{1}{2\sqrt{6}}(2s^\dagger_{\mathbf{xy}} + 2s^\dagger_{\bar{\mathbf{x}}\bar{\mathbf{y}}} + 2s^\dagger_{\mathbf{x}\bar{\mathbf{y}}} + 2s^\dagger_{\bar{\mathbf{x}}\mathbf{y}} - s^\dagger_{\mathbf{yz}} \\ &\quad - s^\dagger_{\bar{\mathbf{y}}\bar{\mathbf{z}}} - s^\dagger_{\mathbf{y}\bar{\mathbf{z}}} - s^\dagger_{\bar{\mathbf{y}}\mathbf{z}} - s^\dagger_{\mathbf{xz}} - s^\dagger_{\bar{\mathbf{x}}\bar{\mathbf{z}}} - s^\dagger_{\mathbf{x}\bar{\mathbf{z}}} - s^\dagger_{\bar{\mathbf{x}}\mathbf{z}}). \end{aligned} \tag{B2}$$

So far, we have ignored spin. The fact that the SO interaction is large on the ion implies that the ionic states $|m\rangle$ transform according to some double representation of the cubic point group. Let us assume, for the sake of simplicity, that the ionic ground state multiplet transforms as a $j \sim 3/2$ spin, i.e., according to the Γ_8 double representation, and can hybridize only with nearest neighbor states of the same symmetry. This leads us to the definition of the following operators,

$$\begin{aligned} s^\dagger_{3/2} &= -D^\dagger_{x^2-y^2,\downarrow}, \quad s^\dagger_{-3/2} = D^\dagger_{x^2-y^2,\uparrow} \\ s^\dagger_{1/2} &= D^\dagger_{2z^2-x^2-y^2,\uparrow}, \quad s^\dagger_{-1/2} = -D^\dagger_{2z^2-x^2-y^2,\downarrow}. \end{aligned} \tag{B3}$$

These operators transform also according to Γ_8, and therefore the local part of the ionic Hamiltonian, Eq. (B1), reduces to

$$\mathcal{H}_{\mathrm{LSO}} = E_d \sum_m |m\rangle\langle m| + V \sum_m (|m\rangle\langle 0|s_m + s^\dagger_m|0\rangle\langle m|), \tag{B4}$$

where V is the hybridization parameter, and we choose $E_0 = 0$ and $E_1 = E_d$. Performing a Coqblin-Schrieffer transformation [15,16] for the Hamiltonian Eq. (B4), we finally obtain

$$\mathcal{H}_{\mathrm{LSO}} = J \sum_{m,m'} s^\dagger_m s_{m'} X_{m'm}, \tag{B5}$$

where the Hubbard operators $X_{m'm} = |m'\rangle\langle m|$ refer to the states $\{\frac{3}{2}, \frac{1}{2}, -\frac{1}{2}, -\frac{3}{2}\}$ of the impurity, and $s^\dagger_m$ creates appropriate host electrons, while J denotes the exchange constant $J = \frac{V^2}{|E_d|}$. In our calculations we set J to 0.25 eV, consistent with a Kondo temperature below 0.1 K.

APPENDIX C: MAGNETIC ANISOTROPY IN THE T_2 SPACE

Here we derive the MA matrix from the LSO model. The host Hamiltonian, Eq. (A3), must be modified in the presence of a magnetic impurity. The simplest way to account for the missing host atom at the impurity site is to shift the on-site d-state energies of the impurity ε^i_α far below the valence band by adding the following term to the Hamiltonian,

$$\Delta\hat{H} = \Delta H^{n,n'}_{\alpha\sigma,\alpha'\sigma'} = \left(\varepsilon^i_\alpha - \varepsilon_\alpha\right)\delta_{n0}\delta_{n'0}\delta_{\alpha\alpha'}\delta_{\sigma\sigma'}. \tag{C1}$$

To commute the anisotropy energy within the LSO model, we need the Green's function only for a cluster of sites $\mathcal{C}$ consisting of nearest neighbor atoms around the impurity and the impurity itself (12 + 1 atoms). The corresponding Green's function matrix can be evaluated as

$$\hat{g}(z) = \hat{g}'(z)(\hat{I} - \Delta\hat{H}'\hat{g}(z))^{-1}, \tag{C2}$$

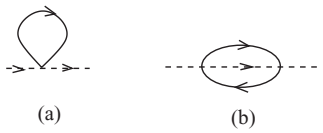

FIG. 5. First- and second-order self-energy diagrams of the impurity spin. The dashed and continuous lines denote the propagators of the spin and the conduction electrons, respectively.

where $\hat{I}$ is a unit matrix and $\hat{g}'(z) = \{\hat{G}(z)\}_{\mathcal{C}}$, and $\hat{G}(z)$ is defined by Eq. (A8). The spectral function matrix of cluster $\mathcal{C}$ is then defined as

$$\hat{\rho}_{\mathcal{C}}(\varepsilon) = -\frac{1}{2\pi i}\lim_{\delta\to 0}[\hat{g}(\varepsilon + i\delta) - \hat{g}(\varepsilon - i\delta)]. \tag{C3}$$

Our impurity model is restricted to the hybridization between the impurity and the s-type conduction electrons, hence, from the s components of the matrix $\hat{\rho}_{\mathcal{C}}(\varepsilon)$ we define the following projected matrix,

$$\rho^{nn'}_{s-\mathcal{C},\sigma\sigma'}(\varepsilon) = \rho^{nn'}_{\mathcal{C},s\sigma,s\sigma'}(\varepsilon), \tag{C4}$$

where n,n' label sites in $\mathcal{C}$ and $\hat{\rho}_{s-\mathcal{C}}$ is a $(2\times 13)\times(2\times 13)$ matrix, incorporating the up ($\uparrow$) and down ($\downarrow$) spin channels, too. Finally, we compute the 4×4 matrix of spectral functions $\rho^{L}_{mm'}(\epsilon)$ of the symmetry-adopted operators $s^{\dagger}_{m}$ from $\hat{\rho}_{s-\mathcal{C}}$ by performing the unitary transformation defined by Eqs. (B2) and (B3).

To calculate the splitting of the four states, we perform second-order permutation theory in J by employing Abrikosov's pseudofermion representation [21]. The corresponding diagrams are shown in Fig. 5. The $T = 0$ temperature pseudofermion self-energy is given by

$$\Sigma_{mm'}(\omega = 0) = \Sigma^{(1)}_{mm'} + \Sigma^{(2)}_{mm'}, \tag{C5}$$

where

$$\Sigma^{(1)}_{mm'} = J\int_{-\infty}^{\varepsilon_F} d\varepsilon \rho^{L}_{mm'}(\varepsilon) \tag{C6}$$

and

$$\Sigma^{(2)}_{mm'} = J^2\int_{-\infty}^{\varepsilon_F} d\varepsilon \int_{\varepsilon_F}^{\infty} d\varepsilon' \frac{1}{\varepsilon' - \varepsilon}\rho^{L}_{mm'}(\varepsilon)\sum_{m''}\rho^{L}_{m''m''}(\varepsilon'). \tag{C7}$$

Here $\rho^{L}_{mm'}(\varepsilon)$ denote the elements of $\rho^{L}(\varepsilon)$ computed in the absence of the exchange interaction, i.e., $J = 0$, and ε_F is the Fermi energy [11]. Interestingly, already the first-order contribution to the self-energy gives a nonvanishing anisotropy in the vicinity of a surface or at a site of a nanograin. Therefore, we consider this leading term only and identify the MA matrix as the first-order self-energy contribution $K_{mm'} = \Sigma^{(1)}_{mm'}$, and express the effective spin Hamiltonian as

$$H^{L} = \sum_{m,m'} K_{mm'}|m'\rangle\langle m|. \tag{C8}$$

As demonstrated in Fig. 6 for a regular cluster of 225 atoms, in an ordered nanograin the MA splitting is the same for sites in the same shell by O_h symmetry relations. Constructing disordered nanograins by placing 40 extra atoms randomly on the next three outermost shells generates widely fluctuation anisotropies within each shell.

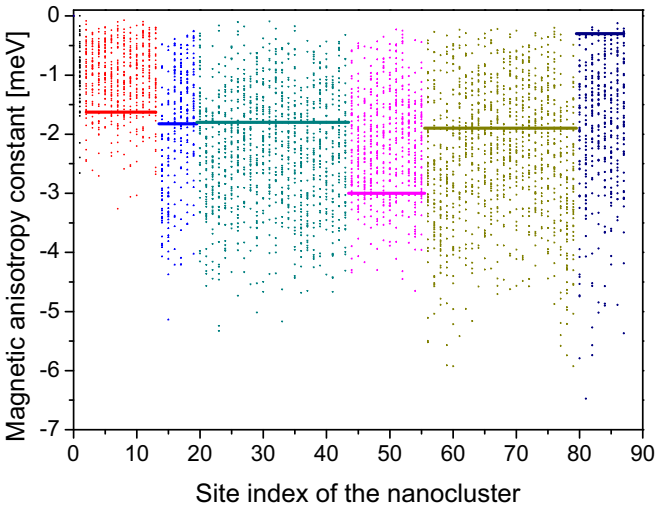

FIG. 6. (Color online) Calculated MA constant K_L values for both ordered and disordered nanoballs. The ordered cluster has $N = 225$ atoms, and the solid lines correspond to the values of K_L calculated for the ordered case. The number of core sites is $N_c = 87$, i.e., the MA is for atoms located in the center site and on the first six core shells—see the different colors. The number of all sites in disordered nanoballs is $N = 265$, i.e., 40 extra atoms are put to the next three outermost shells. The number of sample is $N_S = 50$.

In the case of tetragonal symmetry, when the magnetic impurity is, e.g., in the vicinity of a surface of a film or bulk material, the MA matrix has only diagonal elements, $K_L = K_1$. Moreover, in the case of perfect cubic symmetry, when the magnetic impurity is in the bulk, $K_1 = 0$, too, and therefore $K_L = 0$ as well, implying that the $D^{3/2}$ ground state (Γ_8) remains degenerate. It follows that the magnetic anisotropy should go to zero in the inner shells upon increasing the size of the nanograins. Indeed, the characteristic MA energy vanishes as $N^{-3/2}$. We remark that in ordered nanoclusters $K_L = 0$ is obtained for the central atom, in agreement with this symmetry analysis.

In ordered grains, the MA matrix is different at each site, however, symmetry relations exist between the MA parameters of atoms on the same shell. Let i and j label two sites within the same shell and let us assume, e.g., that the two sites are connected by a rotation of angle ϕ around axis $\mathbf{n}$. Then the anisotropy matrices H^{L}_{i} and H^{L}_{j} are related by linear transformations as

$$H^{L}_{j} = e^{i\varphi\mathbf{n}\cdot\mathbf{J}}H^{L}_{i}e^{-i\varphi\mathbf{n}\cdot\mathbf{J}}, \tag{C9}$$

with $\mathbf{J} = (J_x, J_y, J_z)$ denoting the $J = 3/2$ spin operators.

Under cubic symmetry transformations, the quadupolar operators $\{Q_1, Q_2\}$ and $\{Q_3, Q_4, Q_5\}$ transform into each other according to the two-dimensional E and three-dimensional T_2 representations, respectively. Correspondingly, the parameters $\mathbf{K}_E \equiv (K_1, K_2)$ and $\mathbf{K}_T \equiv (K_3, K_4, K_5)$ at sites i and j are related as

$$\mathbf{K}^{j}_{E/T} = \Gamma^{(i\to j)}_{E/T}(g)\mathbf{K}^{i}_{E/T}. \tag{C10}$$

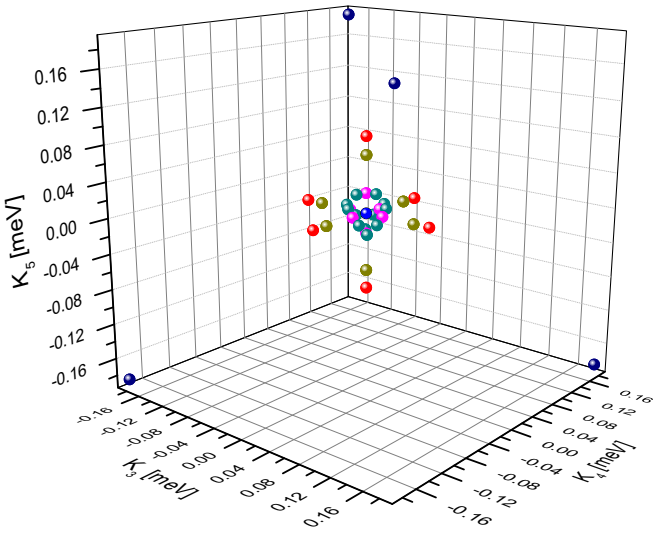

FIG. 7. (Color online) The magnetic anisotropy parameters in the T_2 space in the case of an ordered nanograin ($N = 225$, $N_c = 87$, $N_S = 1$). The color coding is the same as in Fig. 6.

Consequently, the anisotropy parameters of atoms on a given shell form regular structures in the $\mathbf{K}_E$ and $\mathbf{K}_T$ spaces.

Figure 7 shows the MA parameters $\mathbf{K}_T$ in the T_2 space for an ordered nanograin of 225 atoms (87 core atoms). We can clearly identify tetrahedral ordering patterns, in agreement with the structure of the T_2 transformations. The ordered structures can, however, be split even by placing a single extra atom on the outermost shell of the spherical cluster.

The radial distribution of the MA parameters in the T_2 parameter space is shown in Fig. 8 for disordered nanograins. The observed distribution agrees well with the predictions of a simple Gaussian theory, similar to Eq. (6). The scale of the T_2-space anisotropy $\Delta_T \equiv \sqrt{\langle \mathbf{K}_T^2 \rangle}$ is, however, more than one order of magnitude smaller than Δ_E, and vanishes in the absence of bulk SO coupling, $\xi = 0$. The T_2 data in Fig. 8 are distributed similarly to the $\beta = 2$ Gaussian unitary ensemble (GUE).

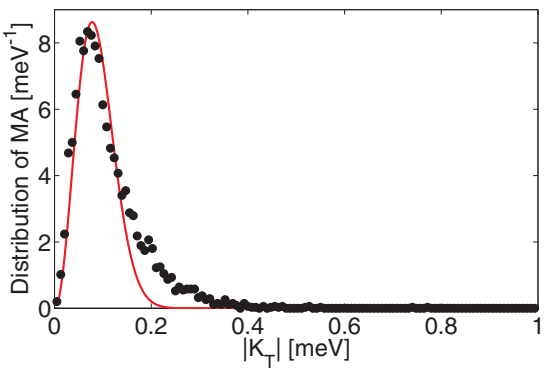

FIG. 8. (Color online) Radial distribution of the magnetic anisotropy parameters (dots) in T_2 space in the case of $N_S = 50$ samples with $N = 225 + 25$ atoms ($N_c = 87$). The continuous line presents the prediction of the Gaussian unitary ensemble. The obtained MA energy scale: $\Delta_T = 0.13$ meV.

APPENDIX D: LEVEL SPACING DISTRIBUTION OF THE HOST

The spectrum of disordered mesoscopic systems is usually analyzed in terms of random matrix theory (RMT). Here we analyze the energy level spacing distribution of the Hamiltonian Eq. (A3) in the presence of host SO coupling. Generically, the matrix $\hat{H}$ of a disordered grain is an $M \times M$ matrix of $M/2$ different Kramers degenerate eigenvalues $\{\varepsilon_i\}$. The level spacing is defined as the separation of two consecutive eigenvalues. Its average over disorder realizations $\langle s \rangle \equiv \Delta$ at an energy ϵ is related to the total DOS of a grain as

$$\Delta(\epsilon) = \frac{1}{2\,\mathrm{DOS}(\varepsilon)}.$$

According to random matrix theory [22], in a chaotic nanograin the distribution of s/Δ is a universal function that depends solely on the symmetry of the underlying Hamiltonian, and is well approximated by Wigner-Dyson statistics,

$$p_\beta(x) = a_\beta\, x^\beta \exp(-b_\beta x^2). \tag{D1}$$

Here β classifies the appropriate symmetry class: In the presence of time reversal symmetry breaking, $\beta = 2$ (and $a_2 = 32/\pi^2$ and $b_2 = 4/\pi$), and one refers to the Gaussian unitary ensemble (GUE), while $\beta = 4$ [with $a_4 = 262\,144/(729\pi^3)$ and $b_4 = 64/(9\pi)$] corresponds to the Gaussian symplectic ensemble (GSE), and describes chaotic systems with SO interaction. The Gaussian orthogonal ensemble (GOE) is characterized by $\beta = 1$.

The distribution of the level spacings for a set of randomly generated $225 + 25$ atom disordered relativistic nanograins with SO coupling $\xi = 0.64$ is shown in Fig. 9. The data presented have been collected from the d band between 3 and 4.5 eV, where the elevated value of the DOS allows a good statistical analysis. Clearly, apart from the tail of the distribution, the data are very well fitted by GSE. Deviations of the level spacing statistics (fat tail) from the predictions of RMT together with the anomalies observed in anisotropy parameter space (angle correlations) may signify that the effect of the cubic symmetry of the underlying lattice is not entirely negligible.

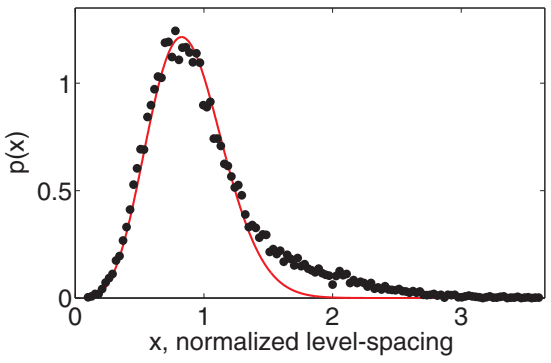

FIG. 9. (Color online) The level spacing distribution for $N_S = 50$ disordered nanograins with $N = 225 + 25$ atoms in the d band. The average level spacing is $\Delta = 3.9$ meV. The data are well fitted by GSE.

APPENDIX E: EXCITATION SPECTRUM OF EMBEDDED MAGNETIC IMPURITIES

The excitation spectra of magnetic impurities embedded in randomly oriented nanograins can be calculated from the effective Hamiltonian H^L, Eq. (5). To describe the spectra of an arbitrarily oriented sample, we rotate H^L by an angle φ around the unit vector $\mathbf{n}$,

$$H^L \to H^L_{\mathbf{n},\varphi} = e^{i\varphi \mathbf{n}\cdot\mathbf{J}} H^L e^{-i\varphi \mathbf{n}\cdot\mathbf{J}}, \tag{E1}$$

with $\mathbf{J} = (J_x, J_y, J_z)$ denoting $J = 3/2$ angular momentum-vector operators. We then solve the eigenproblem of this Hamiltonian, $H^L_{\mathbf{n},\varphi}|i\rangle = E_i|i\rangle$ $(i = 1, \ldots, 4)$. Assuming an ac magnetic field of frequency ω in the x direction, Fermi's golden rule yields for absorbtion intensity

$$S(\omega) \propto \sum_{j>i} \delta(\omega - (E_j - E_i)/\hbar)|\langle j|J_x|i\rangle|^2 p_i, \tag{E2}$$

with $p_i = e^{-\beta E_i}/Z$ the Boltzmann weight of the ith eigenstate, and $Z = \sum_i e^{-\beta E_i}$ is the partition function.

We simulated the excitation spectra of $N = 225 + 40$ atom disordered nanograins by generating 100 random grain configurations and then selecting random grain orientations and impurity positions within the grains at liquid helium temperature, $T = 4.2$ K. The obtained results are shown in Fig. 3.

APPENDIX F: SCHOTTKY ANOMALY OF NANOGRAINS WITH MAGNETIC IMPURITIES

Here we derive the specific heat (heat capacity) of the nanoballs with magnetic impurities. We have seen that the MA matrix has two Kramers degenerate eigenstates with the energy splitting equal to $2K_L$ [see Eq. (4)]. Correspondingly, the specific heat of a given spin is then simply expressed as

$$C = k_B \frac{\partial}{\partial T} T^2 \frac{\partial}{\partial T} \log Z, \tag{F1}$$

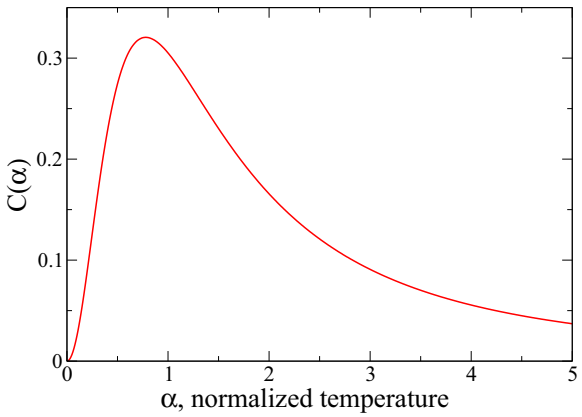

FIG. 10. (Color online) Specific heat (in units of k_B) of nanograins with magnetic impurities, obtained from the numerical integration in Eq. (F4) as a function of the normalized temperature, $\alpha = k_B T/\Delta_E$. This curve is universal for all disordered nanograins, where the MA constants follow a GOE-like universal distribution, Eq. (F3). The grain-specific information is hidden in the parameter Δ_E.

with Z the partition function

$$Z = 2(1 + e^{-2K_L/k_B T}). \tag{F2}$$

Let us now restrict ourselves to the case of E-plane anisotropy. As demonstrated in the main text, the distribution of the MA constant then follows a GOE-type ($\beta = 1$) statistics,

$$p(K_L) = \frac{2}{\Delta_E^2} K_L e^{-K_L^2/\Delta_E^2}. \tag{F3}$$

Averaging the specific heat Eq. (F1) with $p(K_L)$ we then obtain

$$\overline{C(T)} = k_B \alpha^2 \int_0^\infty (12x^2 - 8\alpha^2 x^4) \frac{e^{-\alpha^2 x^2}}{1 + e^{2x}} dx, \tag{F4}$$

where we introduced the normalized temperature $\alpha \equiv \frac{k_B T}{\Delta_E}$. The integral in Eq. (F4) has to be performed numerically, and the result is shown in Fig. 10. The distribution of the MA constants induces a Schottky peak in the specific heat at $\alpha \approx 0.78$, i.e., $T^* \approx 0.78\Delta_E$. We remark that $C(\alpha)$ is proportional to α^2, thus $C(T) \sim T^2/\Delta_E^2$ for temperatures $T \ll T^*$.

[1] *Rare-Earth Permanent Magnets*, edited by J. M. D. Coey (Oxford University Press, Oxford, UK, 1996).

[2] B. Balamurugan, R. Skomski, X. Li, S. Valloppilly, J. Shield, G. C. Hadjipanayis, and D. J. Sellmyer, Nano Lett. **11**, 1747 (2011).

[3] S. Ouazi, S. Vlaic, S. Rusponi, G. Moulas, P. Buluschek, K. Halleux, S. Bornemann, S. Mankovsky, J. Minár, J. B. Staunton, H. Ebert, and H. Brune, Nat. Commun. **3**, 1313 (2012).

[4] S. Andergassen, V. Meden, H. Schoeller, J. Splettstoesser, and M. R. Wegewijs, Nanotechnology **21**, 272001 (2010).

[5] G. Chen and N. Giordano, Phys. Rev. Lett. **66**, 209 (1991).

[6] J. F. DiTusa, K. Lin, M. Park, M. S. Isaacson, and J. M. Parpia, Phys. Rev. Lett. **68**, 1156 (1992).

[7] O. Újsághy, A. Zawadowski, and B. L. Györffy, Phys. Rev. Lett. **76**, 2378 (1996); L. Szunyogh and B. L. Györffy, *ibid.* **78**, 3765 (1997).

[8] A. Szilva, S. Gallego, M. C. Munoz, B. L. Gyorffy, G. Zarand, and L. Szunyogh, Phys. Rev. B **78**, 195418 (2008).

[9] A. Szilva, S. Gallego, M. C. Munoz, B. L. Gyorffy, G. Zarand, and L. Szunyogh, IEEE Trans. Magn. **44**, 2772 (2008).

[10] A. Szilva, Ph.D. thesis, Budapest University of Technology and Economics, 2011.

[11] L. Szunyogh, G. Zaránd, S. Gallego, M. C. Muñoz, and B. L. Györffy, Phys. Rev. Lett. **96**, 067204 (2006); P. W. Brouwer, X. Waintal, and B. I. Halperin, *ibid.* **85**, 369 (2000); D. Davidovic and M. Tinkham, *ibid.* **83**, 1644 (1999).

[12] P. W. Anderson, Phys. Rev. **124**, 41 (1961).

[13] L. L. Hirst, Adv. Phys. **27**, 231 (1978).
[14] M. Tinkham, *Group Theory and Quantum Mechanics* (McGraw-Hill, New York, 1964).
[15] A. C. Hewson, *The Kondo Problem to Heavy Fermions* (Cambridge University Press, Cambridge, UK, 1993).
[16] B. Coqblin and J. R. Schrieffer, Phys. Rev. **185**, 847 (1969).
[17] In the integral defining the MA energy [see Eq. (C6)], a cutoff determined by Δ_{SO} should be, in principle, used. The results presented in the paper are calculated without using a cutoff. However, we checked numerically that by using a cutoff beyond $\Delta_{SO} = 1.5$–2 eV, the MAE does not show significant changes, therefore, our results are relevant to the limit of large $\Delta_{SO}(1.5\ \text{eV})$.
[18] F. Kuemmeth, K. I. Bolotin, S. Shi, and D. C. Ralph, Nano Lett. **8**, 4506 (2008).
[19] M. V. Berry, J. Phys. A: Math. Gen. **10**, 2083 (1977); for a concise review, see, e.g., A. Bäcker, Eur. Phys. J. Spec. Top. **145**, 161 (2007).
[20] L. Szunyogh, B. Újfalussy, P. Weinberger, and J. Kollár, J. Phys.: Condensed Matter. **6**, 3301 (1994).
[21] A. A. Abrikosov, Physics (Long Island City, NY) **2**, 5 (1965).
[22] M. L. Mehta, *Random Matrices* (Elsevier, San Diego, CA, 2004).